Ecosystem Health and Sustainability
A SCIENCE PARTNER JOURNAL

RESEARCH ARTICLE

Unveiling Size-Driven Effects of Silver Nanoparticles on Dissolved Organic Matter and Bacterial Interactions in Lakes

Minshu Cui[1,2†], Chao Zhu[3†], Jinfeng Fang[4], Sanjeeb Mohapatra[5], Yihan Chen[1], Chen-Xuan Li[1], Xiangyu Zhang[1], Min Zhang[3*], Kangping Cui[1], and Xuneng Tong[6,7*]

[1]School of Resources and Environmental Engineering, Hefei University of Technology, Hefei 230009, China. [2]School of Civil Engineering, Hefei University of Technology, Hefei 230009, China. [3]Anhui Ecological and Environmental Monitoring Center, Hefei 230071, China. [4]Betta Pharmaceutical Co., Ltd, Shengzhou, Zhejiang Province 312400, China. [5]Department of Water Management, Delft University of Technology, 2628 CN Delft, the Netherlands. [6]School of Energy and Environment and State Key Laboratory of Marine Pollution, City University of Hong Kong, Hong Kong 999077, China. [7]Department of Civil and Environmental Engineering, National University of Singapore, Singapore 117576, Singapore.

*Address correspondence to: ahhbzhangm@163.com (M.Z.); xunengtong@u.nus.edu (X.T.)
†These authors contributed equally to this work.

Citation: Cui M, Zhu C, Fang J, Mohapatra S, Chen Y, Li CX, Zhang X, Zhang M, Cui K, Tong X. Unveiling Size-Driven Effects of Silver Nanoparticles on Dissolved Organic Matter and Bacterial Interactions in Lakes. *Ecosyst. Health Sustain.* 2025;11:Article 0369. https://doi.org/10.34133/ehs.0369

Submitted 23 January 2025
Revised 30 April 2025
Accepted 25 May 2025
Published 10 June 2025

Lake ecosystems are critical slow-flow environments where silver nanoparticles (AgNPs) and bacterioplankton interact. AgNPs, known for their strong antimicrobial activity and unique physicochemical properties, are widely used across industries but raise environmental concerns due to their size-dependent distinct biochemical effects. Dissolved organic matter (DOM), primarily shaped by microbial activity, constitutes a key organic carbon component in lakes. Understanding DOM turnover under the influence of AgNPs is essential for gaining deeper insights into carbon cycling within lake ecosystems. This study investigated the effects of AgNPs on DOM properties using advanced spectroscopic techniques, highlighting the size-dependent impacts on bacterial community structures and DOM characteristics. Smaller AgNPs exhibited greater microbial toxicity, leading to higher concentrations of protein-associated C1 components within DOM. Furthermore, DOM influenced the transformation of silver between ionic and nanoparticle forms, modulating the toxicity of silver species. AgNPs also enhanced associations between specific bacterial taxa and environmental indicators. Size-dependent effects of AgNPs substantially altered microbial functions related to carbon and nitrogen cycling, affecting bacterial metabolism and the environmental behavior of functional genes. These findings underscore the pivotal role of nanomaterial size in shaping DOM turnover, bacterial community interactions, and biogeochemical processes. Overall, this study provides a foundational understanding of the ecological implications of AgNPs in lake ecosystems and informs future environmental risk assessments.

Introduction

Dissolved organic matter (DOM) comprises thousands of organic compounds primarily derived from plant and animal residues. In aquatic environments, DOM serves as the primary form of organic carbon and functions as a critical nutrient source for microorganisms [1]. Microbial assimilation and respiration collectively alter the composition and properties of DOM, which, in turn, modulates microbial food availability and profoundly impacts the structure and metabolic functions of bacterial communities [2]. Additionally, DOM can originate from the metabolic activity of living bacteria or from the release of organic matter by dead bacteria in aquatic systems [3], emphasizing the importance of understanding the dynamic interactions between DOM and bacterioplankton, regardless of their viability.

Silver nanoparticles (AgNPs) are widely recognized for their antibacterial properties, as well as their exceptional electrical and thermal conductivity [4]. These unique physicochemical properties have made AgNPs valuable across diverse industries, including textiles, catalysis, electronics, and personal care products [5]. However, their widespread use has led to environmental release, bioaccumulation in organisms, and persistence in natural aquatic systems. In areas near discharge points of sewage treatment plants, nanosilver concentrations have been reported as high as 17.9×10^6 to 45.1×10^6 AgNPs/l [6]. Studies indicate that AgNPs exhibit potent antimicrobial effects against various bacterial

strains and viruses. Notably, the size of nanoparticles plays a critical role in their biological interactions, as size-dependent enthalpic and entropic properties govern the adhesive strength between nanoparticles and cellular receptors. This significantly influences cellular uptake pathways [7]. Smaller nanoparticles, in particular, demonstrate a conspicuous positive correlation with heightened cytotoxicity, attributed to their larger surface area and higher proportion of exposed molecules, which enhance interactions with cells [8]. The mechanisms of AgNPs toxicity are multifaceted. One major mechanism involves the oxidative dissolution of AgNPs, releasing Ag^+ ions, which can bind to thiol groups in proteins, disrupt enzyme activity, and damage cellular membranes [9]. Additionally, AgNPs induce the generation of reactive oxygen species, leading to oxidative stress that impairs cellular proteins, lipids, and DNA [10]. AgNPs can also directly interact with intracellular macromolecules, further amplifying their cytotoxic effects [11].

The presence of DOM in aquatic environments can modulate these mechanisms by influencing the transformation, bioavailability, and aggregation behavior of AgNPs. DOM molecules can form coatings around AgNPs, stabilize or destabilize them through steric and electrostatic interactions, and chelate Ag^+ ions, thus affecting both their physical fate and biological effects [12]. For instance, recent findings suggest that natural organic matter can mitigate AgNPs toxicity by reducing ion release and oxidative stress responses in microbial communities [13]. However, the interaction is bidirectional. AgNPs can also alter DOM composition by disrupting microbial metabolism, which may result in the release of proteinaceous or humic-like substances [14]. These findings suggest that AgNPs of varying sizes may exert distinct effects on microorganisms, potentially altering the composition and properties of DOM. Therefore, understanding the size-dependent interactions between AgNPs, microorganisms, and DOM is essential for preserving lake ecosystem functions and accurately predicting carbon cycling dynamics.

Lakes are critical slow-flowing water bodies within watershed environments, where extended hydraulic residence times can amplify the environmental and microecological impacts of AgNPs. This study utilized water samples from Chaohu Lake in laboratory culture experiments with AgNPs of varying particle sizes (5, 50, and 100 nm). Through comprehensive analyses of environmental indicators, DOM composition and properties, and bacterial community structure and functional potential, this research aims to (a) assess the size-dependent effects of AgNPs on DOM dynamics, and (b) elucidate their influence on bacterioplankton communities, including their interactions with key functional genes. By addressing these objectives, this study seeks to provide deeper insights into the ecological consequences of AgNPs pollution in lake ecosystems, thereby offering new insights into the ecological implications of nanoparticle pollution in aquatic environments.

Materials and Methods

Experimental design

Water samples were collected from Chaohu Lake and transported to the laboratory for experimentation. The study consisted of 3 experimental groups and one control group, each with 3 replicates. AgNPs of 3 particle sizes (5, 50, and 100 nm) were obtained from Jiangsu Xianfeng Nanomaterials Technology Co. Ltd., China. The size and morphology of AgNPs were confirmed by scanning electron microscope (SEM) imaging and ultraviolet–visible (UV–Vis) spectroscopy (Figs. S1 and S2). The concentration of AgNPs was set at 0.1 mg/l according to previous studies [15,16]. The 6-day culture experiment was conducted under simulated natural conditions, with dissolved oxygen levels maintained at 6 to 7 mg/l through continuous aeration. All experiments were conducted in an incubator set at 25 ± 1 °C. The initial pH value of the water sample was 7.8 ± 0.1. The systems were exposed to a 12-h light/12-h dark photoperiod using cool white fluorescent lamps to mimic natural sunlight exposure in shallow lakes. The initial total nitrogen, total phosphorus, ammonia nitrogen, nitrate nitrogen, and nitrite nitrogen were 2.31, 0.57, 1.53, 0.76, and 0.15 mg/l, respectively. Samples were collected in 0, 2, 4, and 6 days. Filtrates from the collected samples were analyzed for water quality parameters and DOM composition. Microorganisms retained on the filter membranes were subjected to DNA extraction using the Fast DNA Spin Kit for Soil (MP Biomedicals, USA) and subsequently analyzed for 16S rRNA gene sequencing.

Characterization of water samples

Various water quality parameters, including dissolved organic carbon (DOC), total nitrogen (TN), ammonia nitrogen (NH_3-N), nitrate nitrogen (NO_3-N), and nitrite nitrogen (NO_2-N), were measured following the protocols outlined in the *Methods for Water and Wastewater Monitoring and Analysis* (4th Edition, 2002). DOC concentrations were determined using a total organic carbon (TOC) analyzer. Nitrogen indicators were analyzed using the following methods: UV spectrophotometry for TN, salicylic acid spectrophotometry for NH_3-N, the spectrophotometric method with phenoldisulfonic acid for NO_3-N, and molecular absorption spectrometry for NO_2-N.

The optical properties of DOM were evaluated using UV–Vis absorption spectroscopy and 3-dimensional fluorescence spectroscopy, with corresponding spectral indices calculated. UV–Vis absorption spectra were obtained using an Agilent Cary 60 UV–Vis spectrophotometer (Agilent, USA). Excitation–emission matrices (EEMs) of DOM were generated with a Hitachi F-7000 fluorescence spectrometer. EEM data were subsequently analyzed using parallel factor analysis (PARAFAC) with the Dreemflour toolbox [17].

Intracellular and extracellular DNA extraction

Water samples (300 ml) were filtered through a GF/F filter to separate the membrane (0.22 μm) and filtered water. Intracellular DNA was extracted from the filter membranes using the FastDNA Spin Kit for Soil (MP Bio, USA), following the manufacturer's instructions. Filtered water was centrifuged (10,000 *g*, 4 °C, 30 min), and the supernatants were concentrated and stored on ice for subsequent extracellular DNA extraction, as detailed in previous studies [18]. The sample for extracellular DNA extraction was first added to NaH_2PO_4 (0.12 M, pH 8.0) and polyvinyl polypyrrolidone, followed by centrifugation and filtration, and then processed using the cetyltrimethylammonium bromide method [19]. All the extracted DNA was assessed based on microspectrophotometry using a NanoDrop ND-2000 (Thermo Fisher Scientific, USA). Then, the qualified DNA was adjusted to 30 ng/ml and stored at −80 °C until molecular analysis.

16S rRNA gene sequencing and analysis

Primers targeting the V3–V4 hypervariable regions of the 16S rRNA gene were amplified using the forward primer 341F (5-CCT AYG GGRBGCASCAG-3) and the reverse primer 806R

(5-GGACTACNNGGGGTATCTAAT-3) [20]. The purified amplification products were adjusted to the same concentration for sequencing. Correspondingly, the absolute abundance of 16S rRNA genes was determined using the real-time fluorescence quantitative PCR, and the 16S rRNA high-throughput sequencing was conducted on an Illumina MiSeq PE300 platform (Illumina, San Diego, USA) according to the standard protocols by Majorbio Bio-Pharm Technology Co. Ltd. (Shanghai, China). The qPCR reaction conditions were as follows: an initial denaturation at 95 °C for 2 min, followed by 25 cycles of 95 °C for 30 s, 55 °C for 30 s, and 72 °C for 30 s, with a final extension at 72 °C for 5 min [21]. Bioinformatic analysis of the raw sequencing data was conducted using the Online Cloud Platform (www.i-sanger.com). In order to reduce the PCR operation error of the assay, each sample was performed in triplicate.

Statistical analysis

Species were analyzed at the genus level, excluding those with a relative abundance of less than 0.02% or an occurrence frequency below 20% [22]. Genera meeting these criteria were visualized in a genus-level heatmap. Data analyses were conducted using R (version 4.3.2). The Kruskal–Wallis test was applied to non-normally distributed data to analyze biomass and the Shannon diversity index. Bacterial community composition was assessed using permutational multivariate analysis of variance (PERMANOVA) with 9,999 permutations. Principal coordinate analysis (PCoA) was performed using the "vegan" package in R, while redundancy analysis (RDA) was carried out using Canoco 5. Network analysis was based on Spearman correlations ($r \geq 0.6$, $P \leq 0.05$) and visualized with the Gephi platform (version 0.1.0). Statistical methods and corresponding P value thresholds for specific analyses are detailed in the relevant figure legends and result descriptions. Statistical significance was tested at $P < 0.05$.

Results

Characteristics of DOM by UV–Vis absorbance

During the cultivation of water samples, the DOC concentration fluctuated between 8.22 and 26.98 mg/l, following an overall increasing and then decreasing trend (Fig. 1A). Water samples treated with AgNPs exhibited higher DOC concentrations compared to the control group, with significant differences observed across particle sizes ($P < 0.01$). Absorption coefficients at specific wavelengths quantified the concentration of colored DOM. The absorption coefficient at 254 nm, $a(254)$, indicates DOM abundance in the UVC band, while $a(350)$ at 350 nm reflects abundance in the UVB band, with higher values suggesting greater aromatic content [23].

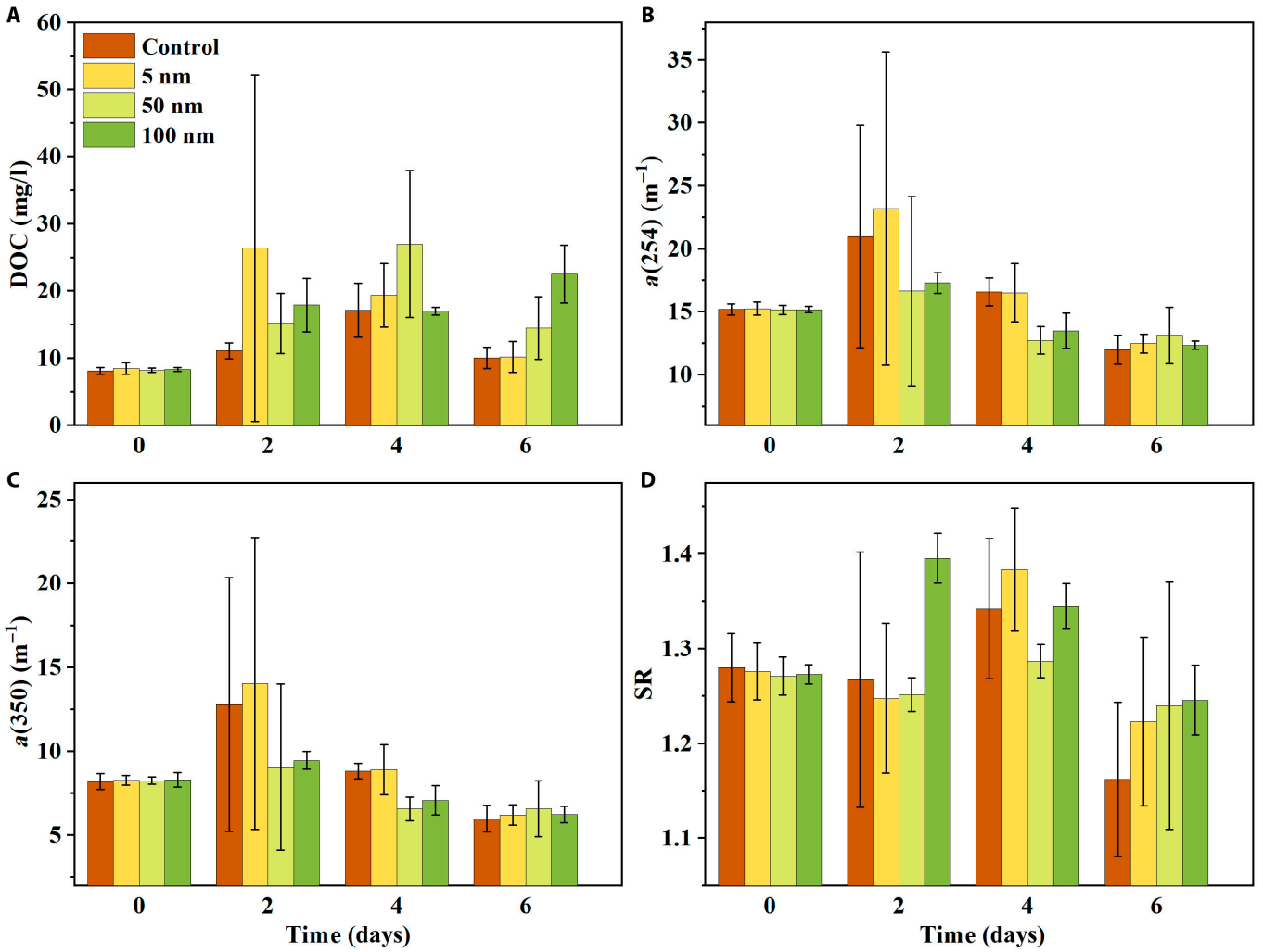

Fig. 1. Effect of AgNPs size on the (A) DOC concentration, (B) absorption coefficient at 254 nm, (C) absorption coefficient at 254 nm, and (D) spectral slope ratio.

Both $a(254)$ and $a(350)$ showed similar trends across all groups, initially increasing and then declining during the experiment (Fig. 1B and C, $P < 0.01$). The 5-nm AgNPs-treated group consistently displayed higher $a(254)$ and $a(350)$ values compared to the control, whereas larger particle sizes corresponded to lower values. The spectral slope ratio (SR), representing changes in the average molecular weight of DOM, also exhibited an increasing and then decreasing pattern over time. Higher SR values indicated a greater prevalence of low-molecular-weight substances and reduced aromaticity [24]. After 6 days, DOM in the AgNPs-treated groups exhibited lower molecular weights compared to the control ($P < 0.05$; Fig. 1D).

Fluorescence indicators provided further insights into DOM characteristics, as illustrated in Fig. 2. The humification index (HIX), an indicator of DOM humification, initially decreased before increasing across all groups. The 50-nm AgNPs-treated group demonstrated elevated HIX values compared to the control; however, the overall HIX range (0.21 to 0.42) suggested limited humification. The fluorescence index (FI), which reflects microbial contributions to DOM, ranged from 1.7 to 1.9 for both treated and control groups, indicating a mix of terrestrial and autochthonous DOM sources. The biological index (BIX), representing the contribution of biological sources to DOM, remained above 1 in all samples, highlighting a strong microbial or biological influence. AgNPs treatments had minimal effects on both BIX and FI values.

PARAFAC analysis of DOM

The EEM spectra of DOM interacting with AgNPs of varying sizes were analyzed using PARAFAC, identifying 3 components through split-half validation, core consistency analysis, and residual analysis (Fig. S3). These components included one protein-like component (C1) and 2 humic-like fluorescence components (C2 and C3). Component C1, located at Ex/Em 280 nm/325 nm, represented a tyrosine-like substance formed through microbial activity [25]. Significant correlations were observed between C1 and $a(254)$ ($P < 0.05$), C1 and $a(350)$ ($P < 0.05$), and C1 and SR ($P < 0.01$). Component C2 was identified as a terrestrial fulvic acid component with an Ex/Em of 250 nm/400 nm [26]. Component C3 exhibited a primary peak at Ex/Em 270 nm/450 nm and a secondary peak at Ex/Em 360 nm/480 nm, corresponding to a UVC-type humic substance [27].

AgNPs induced significant shifts in DOM fluorescence intensity (Fig. 3). The 5-nm AgNPs increased overall fluorescence, whereas 50- and 100-nm AgNPs reduced it. The 5-nm AgNPs exhibited minimal impact on the relative abundance of each component. In contrast, 50- and 100-nm AgNPs increased the relative levels of C2 and C3 while reducing C1. Temporal trends in fluorescent component concentrations remained consistent across all groups. Component C1 initially increased and then decreased, while C2 and C3 followed the opposite pattern, first decreasing and then increasing. Notably, 50- and 100-nm AgNPs accelerated these transformations, advancing the inflection points of the trends.

Characterizations of bacterial community

Significant changes in bacterial biomass were observed following the addition of AgNPs (Fig. 4). Intracellular biomass (J) decreased initially but increased with larger AgNPs sizes. In contrast, extracellular biomass (E) exhibited the opposite trend. Specifically, 100-nm AgNPs increased intracellular biomass compared to the control, while 5- and 50-nm AgNPs elevated extracellular biomass. AgNPs had minimal effects on α-diversity, with the Shannon index showing only minor fluctuations. According to the Kruskal–Wallis test, the size effect of AgNPs caused significant differences in bacterial load between J-control and J-5 nm, between J-5 nm and J-100 nm, and between E-5 nm and E-100 nm ($P \leq 0.05$). However, no significant differences ($P > 0.05$) were observed in the Shannon index across groups due to particle size. Significant differences were detected between J and E groups for both bacterial biomass and the Shannon index, particularly between J-control and E-control, and between J-100 nm and E-100 nm ($P \leq 0.05$).

A heatmap of genus-level bacterial relative abundance (Fig. S4) revealed that AgNPs significantly altered the structure of intracellular and extracellular bacterial communities. PCoA supported this observation, with significant separation confirmed by a one-way PERMANOVA test based on Bray–Curtis distances ($R^2 = 0.35$, $P = 0.001$) (Fig. 5). PCoA plots showed distinct separation among different AgNPs sizes within the intracellular group (Fig. 5A, $R^2 = 0.88$, $P = 0.001$), whereas the effect on the extracellular community was less pronounced (Fig. 5B, $R^2 = 0.44$, $P = 0.006$).

Correlation network analysis examined the interactions among DOM indices, nitrogen indices, and bacterial communities influenced by AgNPs of varying sizes. Positive interactions within the network suggested cooperative bacterial assembly, while negative interactions indicated competitive dynamics [28]. Environmental indicator correlations were predominantly positive, except for the HIX and C1, which exhibited a negative relationship (Fig. 6). The intracellular group demonstrated more complex associations, with 55% positive correlations, compared to 62% in the extracellular

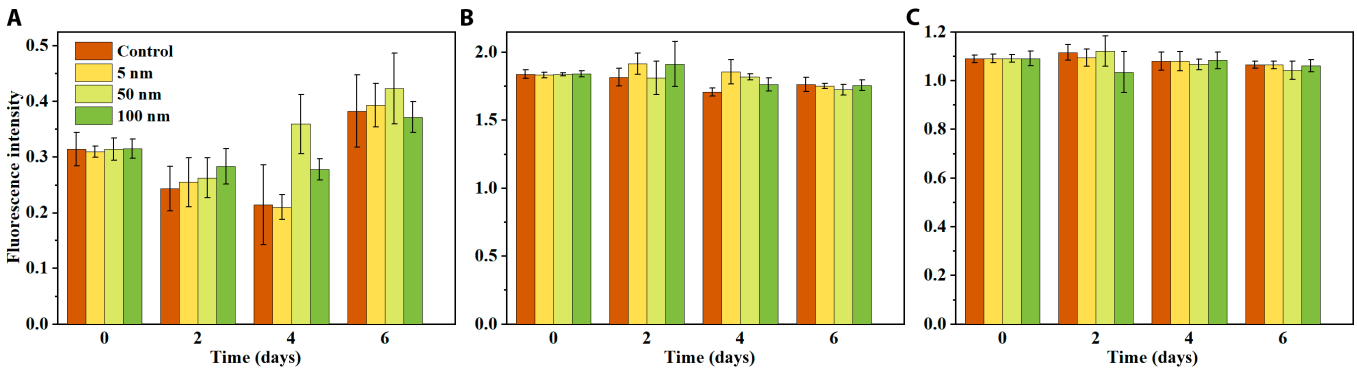

Fig. 2. Fluorescence indicators of DOM under different conditions: (A) humification index; (B) fluorescence index; (C) biological index.

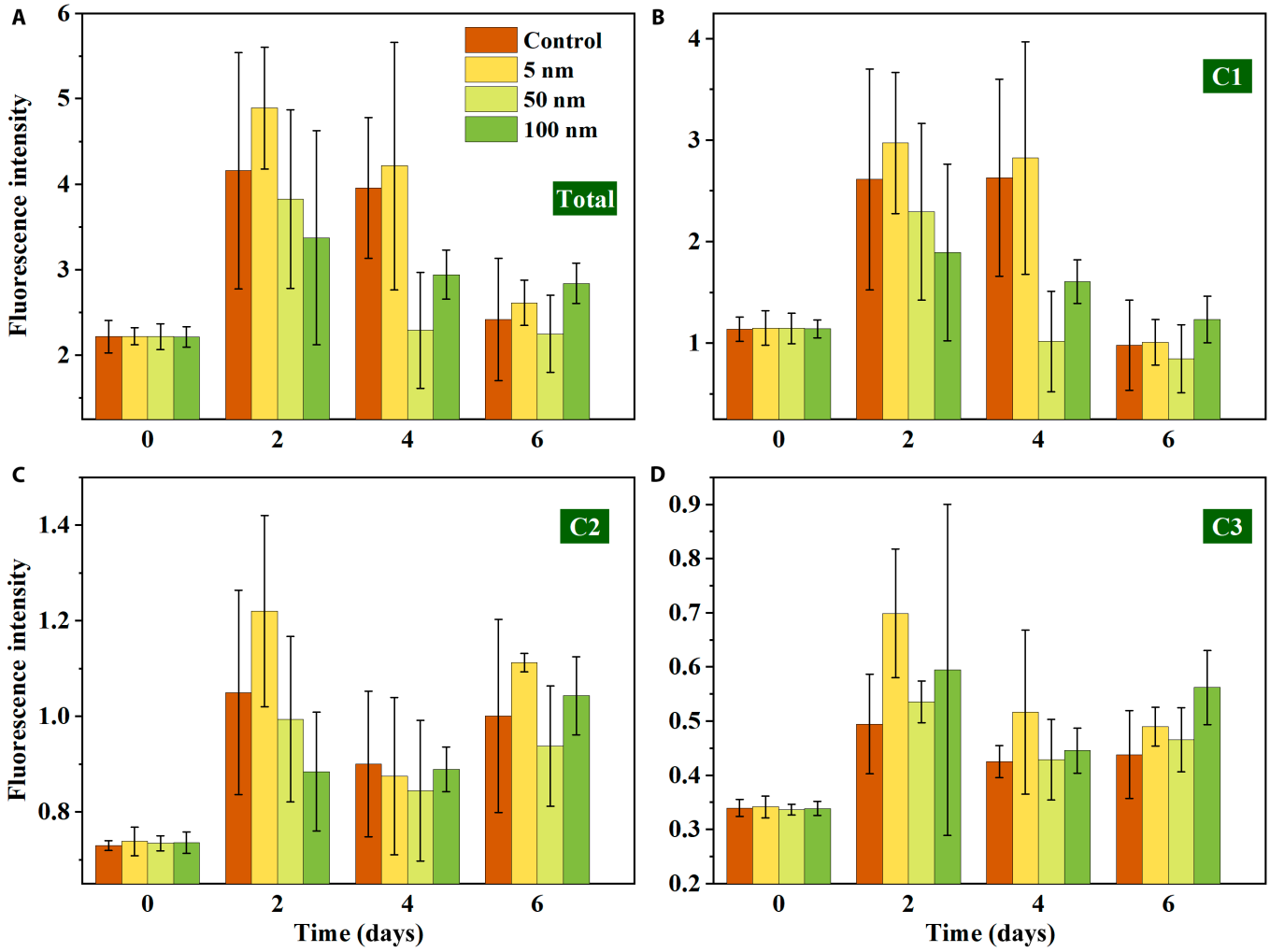

Fig. 3. Fluorescence intensity of each component under different conditions. (A) Total fluorescence intensity, (B) C1 component, (C) C2 component, and (D) C3 component.

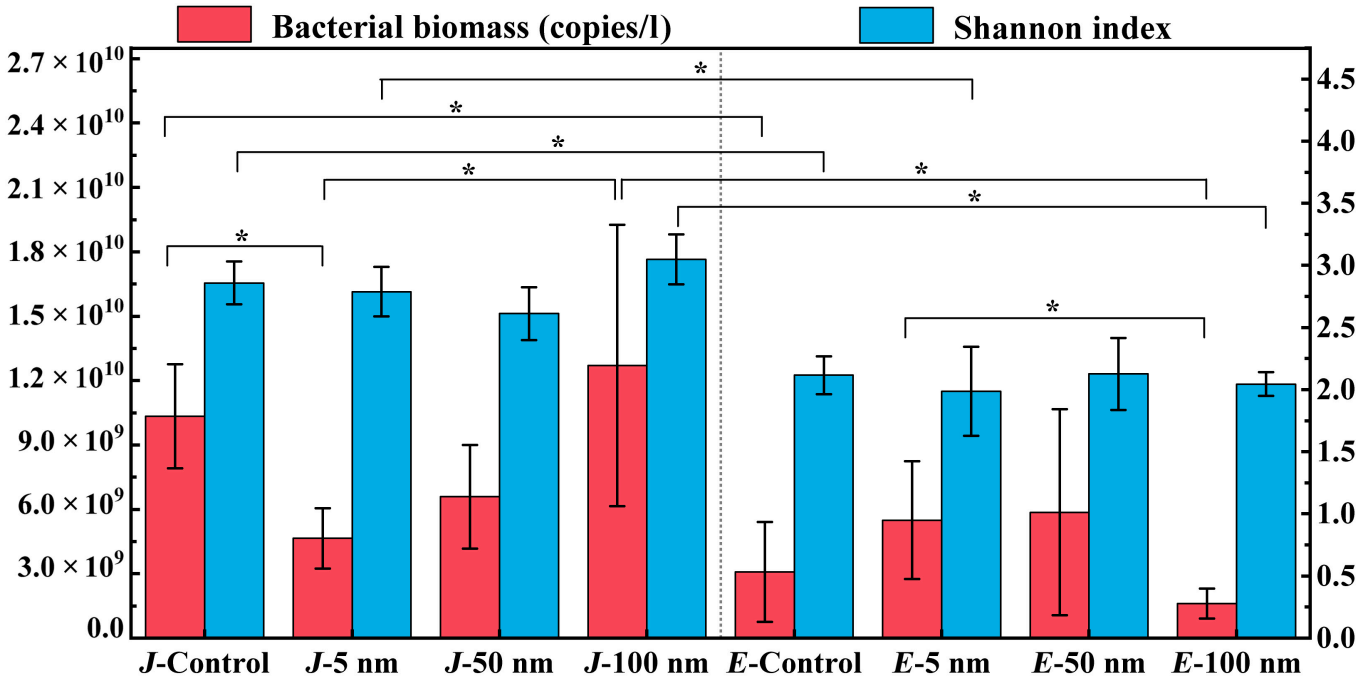

Fig. 4. Bacterial biomass and Shannon index of intracellular (*J*) and extracellular (*E*) bacteria, Kruskal–Wallis test, $*0.01 < P \leq 0.05$.

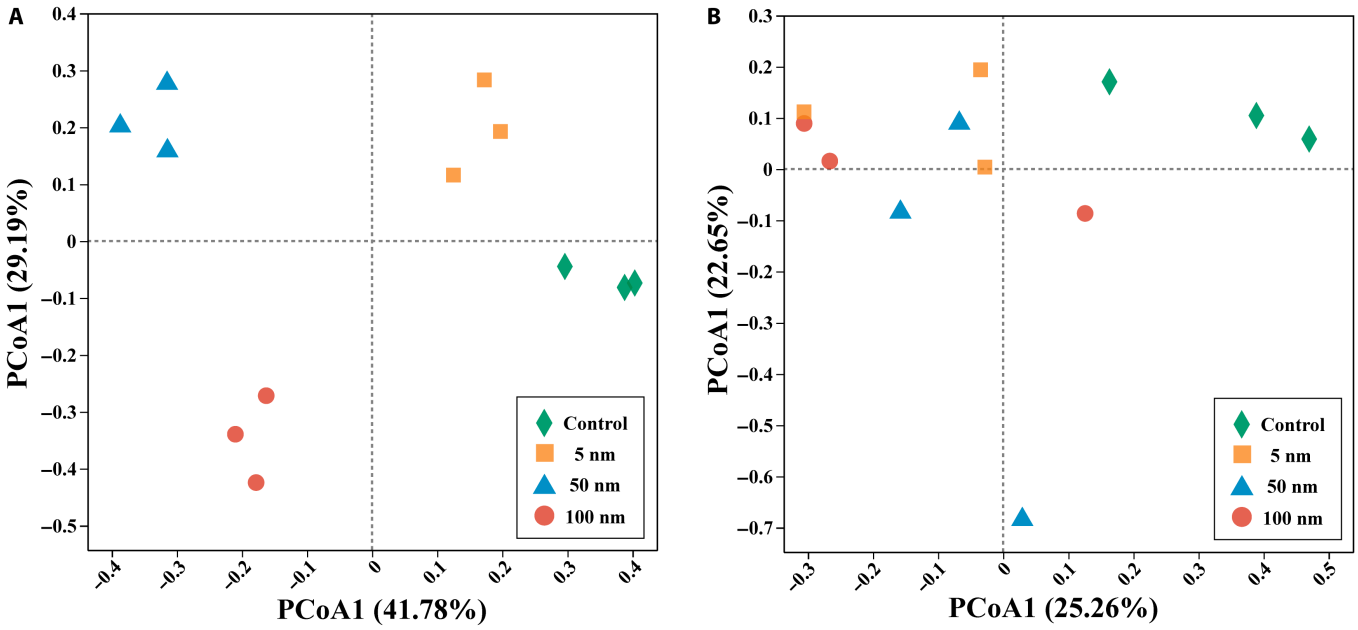

Fig. 5. Principal coordinate analysis of intracellular (A) and extracellular (B) bacterial community. One-way PERMANOVA test based on Bray–Curtis distances ($R^2 = 0.35$, $P = 0.001$).

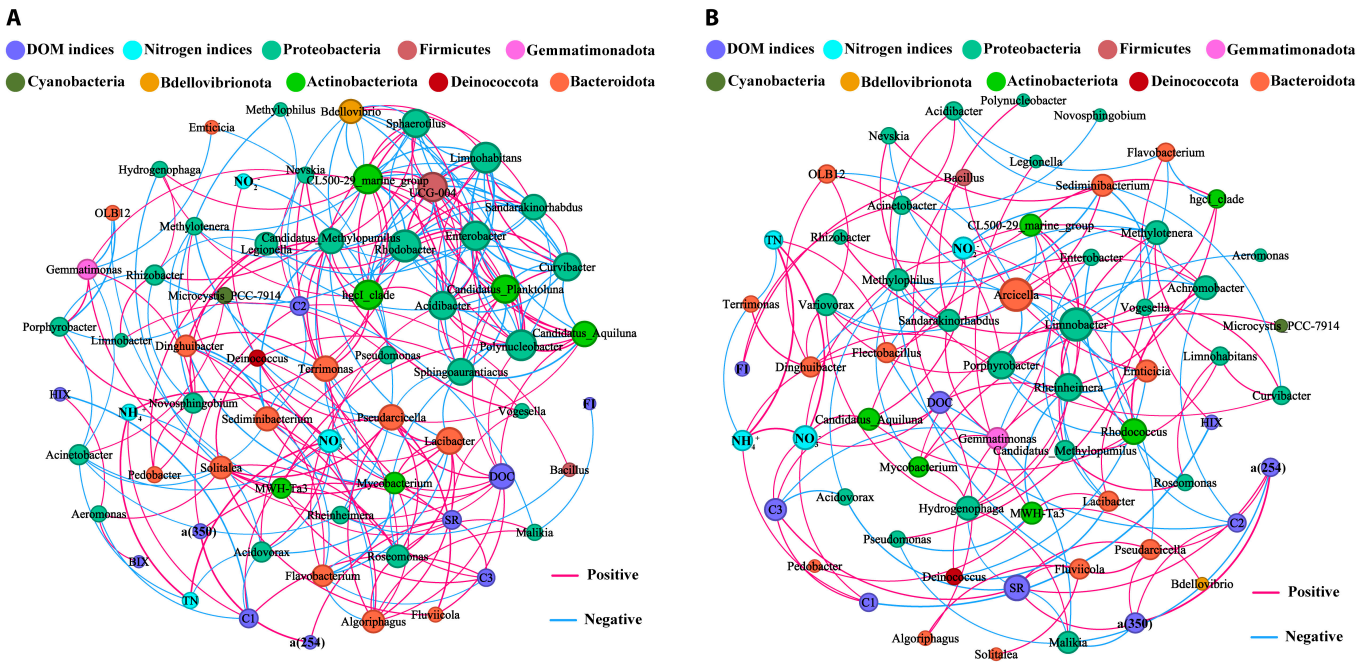

Fig. 6. Correlation network analysis of intracellular (A) and extracellular (B) bacteria at the genus level.

group. AgNPs not only altered bacterial community composition but also strengthened interactions between water quality indicators and bacterial species. The intracellular bacterial community displayed distinct patterns: Actinobacteriota correlated positively with DOM and nitrogen indices, Bacteroidota showed negative correlations with C2 and C3 but positive associations with DOC, and Proteobacteria exhibited positive relationships with most DOM indices, except for C1 and the FI. The extracellular group displayed less clear patterns, with Actinobacteriota and Bacteroidota mostly showing positive associations with DOM and nitrogen indices, while Proteobacteria tended toward negative correlations with DOM indices. *Aeromonas* and *Malikia* exhibited the strongest associations with DOM indices in the intracellular and extracellular groups, respectively, while *Acidovorax* and *Flectobacillus* were most correlated with nitrogen indices.

FAPROTAX was used to predict potential microbial functional genes related to carbon and nitrogen cycles and to assess the impact of DOM characteristics under varying AgNPs sizes. Intracellular denitrification genes were negatively correlated with C1 and C3, while aromatic compound degradation genes showed a negative relationship with C3 (Fig. S5). For extracellular DNA, nitrogen cycle function genes were positively

correlated with SR and C3 but negatively correlated with DOC. Carbon cycle genes displayed positive associations with FI and DOC but inverse relationships with HIX. RDA further explored microbial functional relationships with DOM indicators (Fig. S6). For intracellular DNA, FI, BIX, and HIX showed the strongest positive correlations with genes related to the tricarboxylic acid (TCA) cycle, nitrogen fixation, and acetyl-CoA carboxylase (ACC) functions, respectively. In contrast, C2 displayed the most negative correlations with TCA cycle and nitrogen fixation genes, while NH_4^+ exhibited a notable negative relationship with ACC genes. For extracellular DNA, FI was the most positively correlated indicator for TCA cycle and ACC genes, while BIX positively correlated with nitrogen fixation genes. Conversely, BIX, *a*(350), and HIX were the most negatively associated with TCA cycle, nitrogen fixation, and ACC genes, respectively. Among environmental factors, DOC and TN were strongly associated with the variation in the abundance of certain microbial functional genes, suggesting potential links between nutrient levels and microbial community functions.

Discussion

Different sizes of AgNPs exhibited varying effects on microorganisms. Mechanistically, the antimicrobial activity of AgNPs has been linked to multiple pathways. First, the surface of AgNPs is easily oxidized by oxygen in environmental and biological systems, releasing Ag^+. Ag^+ ions can interact with thiol groups in cellular proteins, impairing enzyme function and membrane permeability [29]. Second, the nanoparticles themselves can attach to or be taken up by cells and induce the generation of reactive oxygen species, resulting in oxidative stress, lipid peroxidation, and DNA damage. Under identical concentration, AgNPs and Ag^+ exhibit differential toxicity toward various microorganisms [30]. Consequently, the toxicity of AgNPs to bacterial communities is primarily mediated through 2 forms: ionic and nanoparticle toxicity [31]. Although the average dissolved oxygen concentrations were similar across experimental groups, the relatively larger specific surface area of smaller AgNPs facilitated oxidation reactions, releasing more Ag^+. Smaller nanoparticles are also more readily absorbed by cells. Previous studies have shown that nanoparticles with diameters of 50 nm or less are more efficiently taken up by cells via endocytosis, with higher absorption rates and intracellular concentrations compared to larger particles [32]. Furthermore, live cells possess nuclear pore complexes on their nuclear envelopes, typically ranging from 20 to 50 nm in diameter. Nanoparticles must be sufficiently small to traverse these pores and enter the nucleus [33]. Once inside the cell, AgNPs act as secondary sources of Ag^+, leading to combined ionic and nanoparticle toxicity, resulting in oxidative stress and direct DNA damage, thereby exhibiting stronger toxic effects [34]. Additionally, AgNPs smaller than 20 nm can elevate intracellular ROS levels and induce apoptosis, whereas nanoparticles larger than 40 nm do not demonstrate this effect [35]. This explains why 5 nm showed stronger toxicity toward bacterial communities, reflected in the significant reduction of intracellular biomass in samples treated with these particles compared to those treated with 100-nm AgNPs (Fig. 4). Similar findings were also reported by Das et al., who observed a significant decrease in bacterial metabolic activity in natural waters after exposure to 1- to 10-nm AgNPs [36]. In addition, studies suggested that other nanomaterials including Fe [37], CeO_2 [38], ZnO [39], and polycyclic aromatic hydrocarbons [40] also exhibited negative effect toward microbial activity and human health risk. In addition to 5 nm, 50-nm AgNPs also showed toxicity toward bacterial communities, possibly due to the abovementioned reasons.

The toxicity of AgNPs fundamentally influenced bacterial metabolism and survival, continuously shaping the chemodiversity of DOM by transforming DOM molecules and generating new organic substances. Statistical analyses and spectroscopic results demonstrated that AgNPs particle size significantly affected DOM turnover. DOC concentrations were strongly correlated with AgNPs size (Fig. 1A). Combined with the results of SR, in the early stages of cultivation, 100-nm AgNPs promoted the formation of low-molecular-weight DOM, while 5-nm AgNPs accelerated DOM aggregation (Fig. 1D). These patterns aligned with changes in C2, the refractory humic-like DOM component (Fig. 3). Variations in refractory DOM components, which are resistant to microbial oxidation, affected the availability of carbon sources, thereby influencing microbial community activity [41].

DOM also played a crucial and dynamic role in modulating the environmental behavior and biological effects of AgNPs. On one hand, DOM facilitated the reduction of Ag^+ to Ag^0, decreasing the toxicity of silver species to microorganisms. On the other hand, experimental results also evidenced that the AgNPs toxicity was associated with the dissolved silver [42]. DOM reduced the solubility of AgNPs, thereby limiting microbial contact and cellular uptake [43]. A similar phenomenon has also been observed in a CuO nanoparticle system, in which humic acid alleviated the toxicity of nanomaterials toward microbes [44]. It should be pointed out that in this closed experimental system, DOM was not externally added but continuously generated through microbial metabolic activity and cell lysis, which were themselves affected by AgNPs exposure. AgNPs of different particle sizes exhibited size-dependent toxicity profiles (Fig. 4). Results showed that 5-nm AgNPs caused the most acute microbial inhibition, resulting in extensive microbial death and a sharp increase in DOC concentration. This newly released DOM exerted a protective effect by decreasing Ag^+ availability and nanoparticle–cell interactions, as reflected in the subsequent DOC decline due to microbial recovery, respiration, and assimilation (Fig. 1A). In contrast, 100-nm AgNPs showed milder but more persistent toxicity, as evidenced by a gradual DOC increase over time. Kennedy et al. [45] observed the same phenomenon that the decrease in toxicity due to DOC was more pronounced for AgNPs with smaller sizes. These results demonstrate a dynamic feedback loop. AgNPs size affects microbial activity, which regulates DOM quantity and quality; the DOM, in turn, modulates Ag speciation and toxicity. This interplay highlights that the observed size-dependent changes in DOM composition are not merely passive consequences of AgNPs presence, but rather the result of complex, biotically mediated interactions between nanoparticles, microorganisms, and DOM.

Correlation network analysis revealed that intracellular bacteria exhibited distinct positive or negative associations with various DOM and nitrogen indices at the genus level under the influence of AgNPs at varying sizes (Fig. 6). This phenomenon is aligned with previous work, which suggested that the accumulation of AgNPs had adverse effects on nitrifying bacteria, and consequently influenced the nitrogen transformation [30]. Carbon and nitrogen, as essential nutrients, influenced bacterial growth, with different microbes displaying distinct preferences for specific sources. This resulted in competitive and complementary dynamics within the community. Previous studies have

shown that bacterial communities adapt to changes in DOM chemodiversity [46]. Initially, they metabolize low-molecular-weight (labile) DOM and gradually evolve to efficiently utilize high-molecular-weight (refractory) DOM. Therefore, the size effect of AgNPs on DOM composition and properties significantly influenced the evolution of microbial communities.

AgNPs also impacted bacterial metabolic functions, which varied with particle size (Fig. 3B). For instance, the fluorescence intensity of C1, associated with proteins, was higher in the 5-nm AgNPs group compared to the control. Two mechanisms may explain this observation: bacterial communities may produce protein detoxifiers to mitigate heavy metal toxicity, or AgNPs-induced cell death may release intracellular proteins into the environment [47]. Both mechanisms likely contributed to the increased C1 content in water containing AgNPs. Interactions between the environment and bacterial communities also influenced ecosystem functions. Bacterial communities and their intracellular functional genes regulate carbon and nitrogen cycles, contributing to DOM formation and turnover in aquatic systems. AgNPs changed some key enzymes and genes involved in nitrogen cycling, which potentially resulted in non-negligible changes in the nitrogen cycling in lakes [48]. In addition, AgNPs would disrupt the decomposition process of organic matter in the water environment [49]. Correlation network analysis and RDA suggested that intracellular bacterial functions were influenced by environmental factors and DOM indices, particularly in the presence of AgNPs of varying sizes. For extracellular functional genes, DOM and nanomaterials likely affected free functional genes immediately, which may transfer through processes like conjugation, transformation, or transduction, thereby altering extracellular functions. Furthermore, the reactive oxygen species produced by DOM under sunlight, mainly singlet oxygen and hydroxyl free radicals, induced intracellular oxidative stress and increased cell membrane permeability, thereby indirectly promoting the cell's ability to take up and integrate extracellular DNA, finally inducing bacterial transformation [50]. Together, these interactions shaped microbial community evolution and DOM turnover, while DOM characteristics influenced the environmental behavior of extracellular functional genes.

In this closed research system, microorganisms served as the sole source of DOM, which, in turn, provided essential nutrients for microbial growth. AgNPs of varying particle sizes exhibited distinct toxic effects on microorganisms, significantly influencing their metabolism and survival. By transforming DOM molecules and generating new organic substances, microbes in aquatic environments continuously shape DOM chemodiversity. Meanwhile, DOM properties influenced AgNPs toxicity and nutrient dynamics, thereby impacting microbial diversity and functional genes. Overall, the size effect of AgNPs played a critical role in shaping DOM characteristics and microbial communities in lake water.

Conclusion

This study examined the size-dependent impacts of AgNPs on the dynamics of DOM and bacterial communities in a controlled system, offering valuable insights into nanomaterial behavior in aquatic environments. Smaller AgNPs (5 and 50 nm) exhibited significant toxicity to bacterioplankton due to their higher specific surface area, with 5-nm AgNPs demonstrating the strongest and most rapid effects. These toxic effects resulted in significant reductions in intracellular bacterial biomass and diversity (up to 30% decrease in Shannon index), accompanied by increased extracellular DOM due to microbial death and lysis. In contrast, 100-nm AgNPs showed milder but more prolonged effects, leading to slower DOC accumulation and community shifts. The observed variations in DOM characteristics (e.g., higher contribution of protein-like C1 components under small-sized AgNPs exposure) were driven by microbial feedback responses, including death, metabolism, and potential recovery. Importantly, the results demonstrated a dynamic interaction where AgNPs size modulates microbial structure and activity, which, in turn, regulated DOM production and transformation. DOM not only was a passive product of microbial response, but also actively modulated AgNPs toxicity by affecting silver species availability and microbial exposure. This bidirectional relationship suggested a dynamic feedback loop, in which AgNPs reshaped microbial communities, in turn altering DOM structure and re-regulating AgNPs behavior and toxicity. These findings provided new insights into nanoparticle–microbe–DOM interactions and highlighted the importance of particle size in assessing the ecological risks of nanomaterials. Future research should focus on more complex environmental scenarios (e.g., multi-pollutant systems and varying nutrient conditions), as well as monitoring the transformation of Ag species, to better predict the impact and mechanism of AgNPs in natural aquatic environments.

Acknowledgments

Funding: This work was supported by the National Natural Science Foundation of China (42307299), the Open Project of State Key Laboratory of Urban Water Resources and Environment (ES202124), the China Postdoctoral Science Foundation (2023M730899), and Fundamental Research Funds for the Central Universities (JZ2023HGQB0155). X.T. is also supported by Start-up Grant for New Faculty from the City University of Hong Kong.

Author contributions: M.C.: Conceptualization, methodology, investigation, funding acquisition, and writing—original draft. C.Z.: Resources, investigation, validation, and data curation. C.-X.L.: Formal analysis, validation, and methodology. X.Z.: Software, formal analysis, and investigation. J.F.: Writing—review and editing. S.M.: Writing—review and editing. Y.C.: Conceptualization, project administration, supervision, and funding acquisition. K.C.: Validation and supervision. M.Z.: Resources, project administration, and supervision. X.T.: Conceptualization, supervision, and writing—review and editing.

Competing interests: The authors declare that they have no competing interests.

Data Availability

The data supporting the findings of this study are available upon request.

Supplementary Materials

Figs. S1 to S6

References

1. Ren H, Wang G, Ding W, Li H, Shen X, Shen D, Jiang X, Qadeer A. Response of dissolved organic matter (DOM) and microbial community to submerged macrophytes restoration in lakes: A review. *Environ Res*. 2023;17(Pt 2):Article 116185.

2. Cathalot C, Roussel EG, Perhirin A, Creff V, Donval JP, Guyader V, Roullet G, Gula J, Tamburini C, Garel M, et al. Hydrothermal plumes as hotspots for deep-ocean heterotrophic microbial biomass production. *Nat Commun*. 2021;12(1):Article 6861.
3. Mohapatra S, Sharma N, Mohapatra G, Padhye LP, Mukherji S. Seasonal variation in fluorescence characteristics of dissolved organic matter in wastewater and identification of proteins through HRLC-MS/MS. *J Hazard Mater*. 2021;413:Article 125453.
4. Li H, Xu H. Mechanisms of bacterial resistance to environmental silver and antimicrobial strategies for silver: A review. *Environ Res*. 2024;26:Article 118313.
5. Islam MA, Jacob MV, Antunes E. A critical review on silver nanoparticles: From synthesis and applications to its mitigation through low-cost adsorption by biochar. *J Environ Manag*. 2021;281:Article 111918.
6. Sanchís J, Jiménez-Lamana J, Abad E, Szpunar J, Farré M. Occurrence of cerium-, titanium-, and silver-bearing nanoparticles in the Besòs and Ebro Rivers. *Environ Sci Technol*. 2020;54(7):3969–3978.
7. Vardakas P, Chatziloizou M, Kouretas D. Nanomaterials: Applications, health implications and environmental risks. *Environ Res*. 2024;14(Pt 3)):Article 118706.
8. Jiang W, Kim BY, Rutka JT, Chan WC. Nanoparticle-mediated cellular response is size-dependent. *Nat Nanotechnol*. 2008;3(3):145–150.
9. Liu J, Sonshine DA, Shervani S, Hurt RH. Controlled release of biologically active silver from nanosilver surfaces. *ACS Nano*. 2010;4(11):6903–6913.
10. Das R, Kanchanapally R, Pramanik A, Chakravarty S, Ray PC. Interaction of silver nanoparticles with serum proteins and implications in antimicrobial activity. *Colloids Surf B Biointerfaces*. 2012;89:70–74.
11. Lok CN, Ho CM, Chen R, He QY, Yu WY, Sun H, Tam PKH, Chiu JF, Che CM. Proteomic analysis of the mode of antibacterial action of silver nanoparticles. *J Proteome Res*. 2006;5(4):916–924.
12. Shang Y, Zhang Y, Wang X, Liu L, Wang S. Influence of silver nanoparticles on DOM degradation and microbial community structure. *Water Res*. 2020;169:Article 115254.
13. Navarro E, Baun A, Behra R, Hartmann NB, Filser J, Miao AJ, Quigg A, Santschi PH, Sigg L. Environmental behavior and ecotoxicity of engineered nanoparticles to algae, plants, and fungi. *Ecotoxicology*. 2008;17(5):372–386.
14. Fabrega J, Luoma SN, Tyler CR, Galloway TS, Lead JR. Silver nanoparticles: Behaviour and effects in the aquatic environment. *Environ Int*. 2009;37(2):517–531.
15. Bondarenko O, Juganson K, Ivask A, Kasemets K, Mortimer M, Kahru A. Toxicity of ag, CuO and ZnO nanoparticles to selected environmentally relevant test organisms and mammalian cells in vitro: A critical review. *Arch Toxicol*. 2013;87(7):1181–1200.
16. Fabrega J, Renshaw JC, Lead JR. Interactions of silver nanoparticles with pseudomonas putida biofilms. *Environ Sci Technol*. 2009;43(23):9004–9009.
17. Aftab B, Hur J. Fast tracking the molecular weight changes of humic substances in coagulation/flocculation processes via fluorescence EEM-PARAFAC. *Chemosphere*. 2017;178: 317–324.
18. Mao D, Luo Y, Mathieu J, Wang Q, Feng L, Mu Q, Feng C, Alvarez PJ. Persistence of extracellular DNA in river sediment facilitates antibiotic resistance gene propagation. *Environ Sci Technol*. 2014;48(1):71–78.
19. Zhang S, Medina JS, Wang T, Augsburger N, Al-Gashgari B, Hong PY. Extracting cell-free extracellular DNA from wastewater: Evaluation of extraction protocols for use in complex matrices. *J Hazard Mater Adv*. 2024;13:Article 100400.
20. Wu D, Xu Z, Min S, Wang J, Min J. Characteristics of microbial community structure and influencing factors of Yangcheng Lake and rivers entering Yangcheng Lake during the wet season. *Environ Sci Pollut R*. 2024;31(6):9565–9581.
21. Sun Z, Li G, Wang C, Jing Y, Zhu Y, Zhang S, Liu Y. Community dynamics of prokaryotic and eukaryotic microbes in an estuary reservoir. *Sci Rep*. 2014;4(1):Article 6966.
22. Zhang Z, Yang J, Feng Q, Chen B, Li M, Liang C, Li M, Li Z, Xu Q, Zhang L, et al. Compositional and functional analysis of the microbiome in tissue and saliva of oral squamous cell carcinoma. *Front Microbiol*. 2019;10:Article 1439.
23. Bai Y, Zhang S, Mu E, Zhao Y, Cheng L, Zhu Y, Yuan Y, Wang Y, Ding A. Characterizing the spatiotemporal distribution of dissolved organic matter (DOM) in the Yongding River basin: Insights from flow regulation. *J Environ Manag*. 2023;325:Article 116476.
24. Hu A, Li L, Huang Y, Fu QL, Wang D, Zhang W. Photochemical transformation mechanisms of dissolved organic matters (DOM) derived from different bio-stabilization sludge. *Environ Int*. 2022;169:Article 107534.
25. Chen W, Westerhoff P, Leenheer JA, Booksh K. Fluorescence excitation−emission matrix regional integration to quantify spectra for dissolved organic matter. *Environ Sci Technol*. 2003;37:5701–5710.
26. Su Y, Hu E, Feng M, Zhang Y, Chen F, Liu Z. Comparison of bacterial growth in response to photodegraded terrestrial chromophoric dissolved organic matter in two lakes. *Sci Total Environ*. 2017;579:1203–1214.
27. Pan X, Liu J, Zhang D, Chen X, Song W, Wu F. Binding of dicamba to soluble and bound extracellular polymeric substances (EPS) from aerobic activated sludge: A fluorescence quenching study. *J Colloid Interface Sci*. 2010;345(2):442–447.
28. Pan C, Feng Q, Li Y, Li Y, Liu L, Yu X, Ren S. Rare soil bacteria are more responsive in desertification restoration than abundant bacteria. *Environ Sci Pollut Res*. 2022;29(22): 33323–33334.
29. Xiu ZM, Zhang QB, Puppala HL, Colvin VL, Alvarez PJ. Negligible particle-specific antibacterial activity of silver nanoparticles. *Nano Lett*. 2012;12(8):4271–4275.
30. Choi O, Deng KK, Kim NJ, Ross L Jr, Surampalli RY, Hu Z. The inhibitory effects of silver nanoparticles, silver ions, and silver chloride colloids on microbial growth. *Water Res*. 2008;42(12):3066–3074.
31. McShan D, Ray PC, Yu H. Molecular toxicity mechanism of nanosilver. *J Food Drug Anal*. 2014;22(1):116–127.
32. Chithrani BD, Chan WC. Elucidating the mechanism of cellular uptake and removal of protein-coated gold nanoparticles of different sizes and shapes. *Nano Lett*. 2007;7(6):1542–1550.
33. Wente SR. Gatekeepers of the nucleus. *Science*. 2000;288(5470):1374–1377.
34. Lu W, Senapati D, Wang S, Tovmachenko O, Singh A, Yu H, Ray P. Effect of surface coating on the toxicity of silver nanomaterials on human skin keratinocytes. *Chem Phys Lett*. 2010;487(1–3):92–96.

35. Miethling-Graff R, Rumpker R, Richter M, Verano-Braga T, Kjeldsen F, Brewer J, Hoyland J, Rubahn HG, Erdmann H. Exposure to silver nanoparticles induces size-and dose-dependent oxidative stress and cytotoxicity in human colon carcinoma cells. *Toxicol In Vitro*. 2014;28(7):1280–1289.
36. Das P, Williams CJ, Fulthorpe RR, Hoque ME, Metcalfe CD, Xenopoulos MA. Changes in bacterial community structure after exposure to silver nanoparticles in natural waters. *Environ Sci Technol*. 2012;46(16):9120–9128.
37. Barnes RJ, Riba O, Gardner MN, Singer AC, Jackman SA, Thompson IP. Inhibition of biological TCE and sulphate reduction in the presence of iron nanoparticles. *Chemosphere*. 2010;80(5):554–562.
38. Miao L, Wang P, Wang C, Hou J, Yao Y, Liu J, Lv B, Yang Y, You G, Xu Y, et al. Effect of TiO_2 and CeO_2 nanoparticles on the metabolic activity of surficial sediment microbial communities based on oxygen microelectrodes and high-throughput sequencing. *Water Res*. 2018;129:287–296.
39. Londono N, Donovan AR, Shi H, Geisler M, Liang Y. Impact of TiO_2 and ZnO nanoparticles on an aquatic microbial community: Effect at environmentally relevant concentrations. *Nanotoxicology*. 2017;11(9–10):1140–1156.
40. Luo P, Bao LJ, Li SM, Zeng EY. Size-dependent distribution and inhalation cancer risk of particle-bound polycyclic aromatic hydrocarbons at a typical e-waste recycling and an urban site. *Environ Pollut*. 2015;200:10–15.
41. Li W, Wang B, Liu N, Shi X, Yang M, Liu C. Microbial regulation on refractory dissolved organic matter in inland waters. *Water Res*. 2024;262:Article 122100.
42. Gunsolus IL, Mousavi MP, Hussein K, Bühlmann P, Haynes CL. Effects of humic and fulvic acids on silver nanoparticle stability, dissolution, and toxicity. *Environ Sci Technol*. 2015;49(13):8078–8086.
43. Yang X, Jiang C, Hsu-Kim H, Badireddy AR, Dykstra M, Wiesner M, Hinton DE, Meyer JN. Silver nanoparticle behavior, uptake, and toxicity in *Caenorhabditis elegans*: Effects of natural organic matter. *Environ Sci Technol*. 2014;48(6):3486–3495.
44. Miao L, Wang P, Hou J, Yao Y, Liu Z, Liu S. Low concentrations of copper oxide nanoparticles alter microbial community structure and function of sediment biofilms. *Sci Total Environ*. 2019;653:705–713.
45. Kennedy AJ, Chappell MA, Bednar AJ, Ryan AC, Laird JG, Stanley JK, Steevens JA. Impact of organic carbon on the stability and toxicity of fresh and stored silver nanoparticles. *Environ Sci Technol*. 2012;46(19):10772–10780.
46. Zhao Z, Gonsior M, Schmitt-Kopplin P, Zhan Y, Zhang R, Jiao N, Chen F. Microbial transformation of virus-induced dissolved organic matter from picocyanobacteria: Coupling of bacterial diversity and DOM chemodiversity. *ISME J*. 2019;13(10):2551–2565.
47. Giller KE, Witter E, Mcgrath SP. Toxicity of heavy metals to microorganisms and microbial processes in agricultural soils: A review. *Soil Biol Biochem*. 1998;30(10–11):1389–1414.
48. Bao S, Xu J, Tang W, Fang T. Effect and mechanism of silver nanoparticles on nitrogen transformation in water-sediment system of a hypereutrophic lake. *Sci Total Environ*. 2021;761:Article 144182.
49. Yonathan K, Mann R, Mahbub KR, Gunawan C. The impact of silver nanoparticles on microbial communities and antibiotic resistance determinants in the environment. *Environ Pollut*. 2022;293:Article 118506.
50. Liu QH, Yuan L, Li ZH, Leung KMY, Sheng GP. Natural organic matter enhances natural transformation of extracellular antibiotic resistance genes in sunlit water. *Environ Sci Technol*. 2024;58(40):17990–17998.